THE ASTROPHYSICAL JOURNAL, 536:465–480, 2000 June 10

A MULTIGROUP METHOD FOR RADIATION WITH SCATTERING IN THREE-DIMENSIONAL HYDRODYNAMIC SIMULATIONS

R. SKARTLIEN[1]
Institute of Theoretical Astrophysics, P.O. Box 1029, Blindern, N–0315 Oslo, Norway
Received 1999 November 10; accepted 2000 January 26

ABSTRACT

Substantial approximations in the treatment of radiation are still necessary in three-dimensional simulations in order to avoid extremely large computational costs. Solar radiation hydrodynamic simulations in three dimensions have previously assumed local thermodynamic equilibrium (LTE); an assumption that works well in the deep photosphere. This work aims at bringing these simulations a step further by including scattered radiation, with the goal of modeling chromospheres in three dimensions. We allow for coherent isotropic scattering, which alters the thermal structure and wave amplitudes in the chromosphere. Group mean opacity coefficients are used in group mean source functions that contain approximate scattering terms and exact contributions from thermal emissivity. The resulting three-dimensional scattering problem allows for a computationally efficient solution by a new iteration method. We have compared exact wavelength-integrated monochromatic solutions with the corresponding approximate solutions for solar conditions. We find that the total flux divergence obtained from the groups deviates less than 10% from the exact solution. When using these groups rather than the full monochromatic solution, the CPU time is reduced by a factor of about 100 in a test case for solar conditions.

Subject headings: hydrodynamics — methods: numerical — radiative transfer — Sun: atmosphere — Sun: granulation

1. INTRODUCTION

Radiation is important for the structure and dynamics of stellar atmospheres through its influence on the energy, ionization, and momentum balance. For the solar case, the radiative flux divergence is the dominant term in the energy balance, while the radiation force in the momentum balance can be neglected.

Radiation has previously been treated assuming LTE (local thermodynamic equilibrium) in solar three-dimensional or two-dimensional simulations (e.g., Nordlund 1982; Steffen & Muchmore 1988; Steiner et al. 1998). The solar LTE convection simulations of Nordlund and Stein (e.g., Nordlund 1982; Nordlund & Stein 1990) provide excellent agreement with the observed granular structure (Stein & Nordlund 1989; Spruit, Nordlund, & Title 1990; Nordlund & Stein 1991). We would infer, therefore, that the effect of radiative cooling on convection dynamics is sufficiently described when radiation is treated in LTE.

To study the dynamic influence from the convection zone on the convectively stable atmosphere above, we need to extend these convection simulations by including the chromospheric layers. In these layers, the radiation is neither optically thin nor optically thick and LTE fails completely. The radiation couples regions far apart and we have to solve a complex nonlocal, nonlinear problem. The self-consistent chromospheric non-LTE (NLTE) radiation hydrodynamics problem is solvable in plane-parallel atmospheres with present-day computers if only a few ions are treated simultaneously (Carlsson & Stein 1992, 1997).

It is obvious that we need simplifying assumptions in three-dimensions such that the problem becomes computationally and practically tractable on current computers. This paper describes the radiation method we use in extended solar convection-atmosphere simulations (Skartlien 1998; Skartlien, Stein, & Nordlund 2000), but the same concepts are applicable generally to simulations of other astrophysical objects.

The first simplifying assumption we make is that the opacity is independent of the radiation field, such that it can be calculated in thermodynamic equilibrium (from the Boltzmann-Saha equations) and not from the rate equations as in NLTE.

We include scattering, but we assume that the scattering process is coherent and isotropic. In this case, photons do not change wavelength and can be scattered in any direction with equal probability in the scattering event. This is the second approximation.

By using group mean opacities (e.g., Mihalas & Mihalas 1984), we solve a limited number of scattering problems rather than the full set of monochromatic scattering problems. This is the third approximation since group mean opacities do not produce the exact solution of the problem.

To make use of these three approximations we need to have a way of constructing group mean opacities that preserves the main properties of the radiation problem (like total radiative flux divergence). We also need to develop an efficient iteration scheme for the solution of the scattering problem in each opacity group. These two issues are addressed in this paper.

The most restrictive of the approximations above is probably that of coherent scattering. We know that coherent scattering is a poor approximation in the cores of spectral lines where complete frequency redistribution is a much better description. Moreover, the approximation of coherent scattering gives an effective thermalization depth of $L_{\rm th} \approx \epsilon^{-1/2}$, where ϵ is the effective destruction probability in a spectral line. This is to be compared with the larger thermalization depth $L_{\rm th} \approx \epsilon^{-1}$ in the case of complete frequency redistribution in a Doppler broadened line in a

[1] Present address: Joint Institute for Laboratory Astrophysics, Campus Box 440, University of Colorado, Boulder, CO 80309-0440; roarsk@hao.ucar.edu.

static atmosphere (e.g., Mihalas 1978). If Doppler shifts caused by macroscopic velocity fields are taken into account, the thermalization depth may be even larger.

Despite these shortcomings, we still make the approximation of coherent scattering because of computational reasons. As we shall see, coherent scattering makes it possible to devise a method that takes into account scattering effects with only a modest increase in computational effort as compared with LTE (a factor ~ 5). The more realistic case of complete frequency redistribution, on the other hand, would need a large number of frequency points, with an increase in computational effort by at least a factor of 100.

In § 2, we formulate the radiation problem to be solved. The multigroup method and the iteration method are developed in § 3. We describe how the methods are applied to a solar convection and atmosphere simulation in § 4. Using these simulations, we calculate the errors introduced by using group mean opacities in § 5. We also compare the group mean opacity method to a previous LTE method. The results are summarized in § 6.

2. FORMULATION OF THE PROBLEM

This section defines the monochromatic, coherent and isotropic scattering problem. This defines our fundamental problem, which we will solve approximately by using group mean opacities. We also establish our notation in this section.

2.1. *LTE Opacity and Photon Destruction Probability*

We assume that the opacities can be obtained from atomic-level population densities calculated from the Boltzmann/Saha equations. The opacity in this case is therefore only dependent on local quantities, e.g., temperature and density. We denote this approximation as LTE-opacity. This approximation will be valid when the population densities are controlled mainly by collisions (as in the deep photosphere) but also when dealing with resonance lines of majority ionization stages (such as the Lyman lines of neutral hydrogen and the H and K resonance lines from singly ionized calcium).

The monochromatic opacity χ_λ is split into an absorption opacity κ_λ, which includes all processes that convert photons to thermal energy, and a scattering opacity σ_λ, which includes only scattering processes that do not convert photons to thermal energy. The total monochromatic opacity is

$$\chi_\lambda = \kappa_\lambda + \sigma_\lambda ,$$

with units of cross section per volume, $\mathrm{cm}^2\ \mathrm{cm}^{-3}$. For notational clarity, we have omitted the general direction dependency resulting from, e.g., Doppler shifts of opacity profiles. The scattering and absorption opacities have contributions from line and continuum processes

$$\sigma_\lambda = \sigma_\lambda^{\mathrm{l}} + \sigma_\lambda^{\mathrm{c}} ,$$

and

$$\kappa_\lambda = \kappa_\lambda^{\mathrm{l}} + \kappa_\lambda^{\mathrm{c}} .$$

We define the photon destruction probability as the probability of absorption once a photon interacts with lines or continua:

$$\epsilon_\lambda = \frac{\kappa_\lambda}{\chi_\lambda} = \frac{\chi_\lambda^{\mathrm{l}} \epsilon_\lambda^{\mathrm{l}} + \kappa_\lambda^{\mathrm{c}}}{\chi_\lambda} .$$

Here, $\epsilon_\lambda^{\mathrm{l}}$ is the photon destruction probability in lines, which is defined as the probability of absorption once a photon interacts with an atomic transition:

$$\epsilon_\lambda^{\mathrm{l}} = \frac{\kappa_\lambda^{\mathrm{l}}}{\chi_\lambda^{\mathrm{l}}} ,$$

where $\chi_\lambda^{\mathrm{l}} = \kappa_\lambda^{\mathrm{l}} + \sigma_\lambda^{\mathrm{l}}$ is the line opacity.

2.2. *Source Function with Coherent Isotropic Scattering*

We include nonlocal effects only in the radiation transport (not the opacity) by allowing for scattered radiation in the gas emissivity in addition to thermally generated emissivity. We can write the general angular dependent emissivity as

$$\eta_\lambda(\mathbf{\Omega}) = \int_{\lambda'} \int_{\Omega'} R(\mathbf{\Omega}, \mathbf{\Omega}'; \lambda, \lambda') I_{\lambda'}(\mathbf{\Omega}') d\Omega'\, d\lambda' + \kappa_\lambda(\mathbf{\Omega}) B_\lambda ,$$

where $\mathbf{\Omega}$ is the unit vector along the solid angle Ω, $R(\mathbf{\Omega}, \mathbf{\Omega}'; \lambda, \lambda')$ is the redistribution function in angle and wavelength, $I_{\lambda'}(\mathbf{\Omega}')$ the specific intensity, $\kappa_\lambda(\mathbf{\Omega})$ the absorption opacity, and B_λ the Planck distribution.

We now assume that the velocity fields are negligible, such that the opacity contributions are direction independent. We further assume that the scattering processes are coherent and isotropic. We note that coherency implies no leakage of photons between different wavelength bands. This can be represented formally by the redistribution function

$$R(\mathbf{\Omega}, \mathbf{\Omega}'; \lambda, \lambda') = R(\lambda, \lambda') = \frac{\sigma_{\lambda'}}{4\pi} \delta(\lambda - \lambda') ,$$

where $\sigma_{\lambda'}/4\pi$ represents the isotropic (uniform) angular redistribution and the Dirac delta function $\delta(\lambda - \lambda')$ coherency (no wavelength shift in the scattering process). With these assumptions, the emissivity becomes

$$\eta_\lambda = \frac{\sigma_\lambda}{4\pi} \int_{\Omega'} I_\lambda(\mathbf{\Omega}') d\Omega' + \kappa_\lambda B_\lambda = \sigma_\lambda J_\lambda + \kappa_\lambda B_\lambda , \qquad (1)$$

where J_λ is the mean intensity. By definition, the source function is the ratio between emissivity and opacity:

$$S_\lambda \equiv \frac{\eta_\lambda}{\chi_\lambda} = \frac{\sigma_\lambda}{\chi_\lambda} J_\lambda + \frac{\kappa_\lambda}{\chi_\lambda} B_\lambda = (1 - \epsilon_\lambda) J_\lambda + \epsilon_\lambda B_\lambda , \qquad (2)$$

where we have used the definition of photon destruction probability.

2.3. *Transfer Equation, Flux Divergence, and Lambda Operator*

In cases where typical gas velocities are small compared to the speed of light, the transport equation reads

$$\frac{\partial I_\lambda}{\partial r} = \eta_\lambda - \chi_\lambda I_\lambda , \qquad (3)$$

where r is the geometrical distance in the direction of I_λ. Here we have omitted the angular dependency of I_λ for

clarity. This is an integrodifferential equation for our scattering problem since the emissivity is dependent on the angle-integrated intensity by equation (1). Note the fundamental difference for the LTE/no-scattering case where the transport equation is simply a first-order differential equation with no coupling to other rays.

The radiative flux divergence we need for the energy equation is obtained from angle and wavelength integration of the transport equation (eq. [3]):

$$\nabla \cdot \boldsymbol{F} = \int_\lambda \int_\Omega \frac{\partial I_\lambda}{\partial r} \, d\Omega \, d\lambda = \int_\lambda \int_\Omega (\eta_\lambda - \chi_\lambda I_\lambda) d\Omega \, d\lambda \, . \quad (4)$$

In our case, for isotropic opacity and emissivity we get, when integrating over solid angle,

$$\nabla \cdot \boldsymbol{F} = 4\pi \int_\lambda \eta_\lambda - \chi_\lambda J_\lambda \, d\lambda = 4\pi \int_\lambda \chi_\lambda (S_\lambda - J_\lambda) d\lambda \, .$$

2.3.1. *The Problem as an Integral Equation*

Using the transport equation, it can be shown (Rybicki 1984) that the mean intensity is given by

$$J_\lambda(\boldsymbol{r}) = \Lambda(\chi_\lambda)[S_\lambda] = \int_V S_\lambda(\boldsymbol{r}') K_\lambda(\boldsymbol{r}, \boldsymbol{r}') d^3\boldsymbol{r}' \, ,$$

where the kernel function K that defines the Λ-operator is given by

$$K_\lambda(\boldsymbol{r}, \boldsymbol{r}') = \frac{\chi_\lambda(\boldsymbol{r}')}{4\pi l^2} \exp(-\Delta\tau_\lambda) \, , \quad (5)$$

where $l = |\boldsymbol{r} - \boldsymbol{r}'|$ is the distance from the point $\boldsymbol{r}$ where the mean intensity is evaluated to an arbitrary point $\boldsymbol{r}'$. The corresponding optical path length between these points is given by

$$\Delta\tau_\lambda = \int_0^l \chi_\lambda(\boldsymbol{r}') dl \, . \quad (6)$$

We see that the kernel is small for optically thick media. For larger optical path lengths, the kernel spans larger volumes and the mean intensity is nonlocally determined.

We can formulate the radiation problem as an integral equation in the source function (Fredholm equation of the second kind) by using our definition of the source function in equation (2) and the lambda operator:

$$S_\lambda = (1 - \epsilon_\lambda)\Lambda(\chi_\lambda)[S_\lambda] + \epsilon_\lambda B_\lambda \, . \quad (7)$$

This equation is linear since the opacity used in the lambda operator is independent of the radiation field (the solution). In principle, we could solve this equation numerically by representing the lambda operator as a matrix. The matrix would consist of the discretized kernel function and include N^2 elements where N is the number of grid points. A serious problem arises in three dimensions. For a simulation with 100 grid points in each direction, we would have to deal with $N = 10^6$ unknowns and $N^2 = 10^{12}$ matrix elements. The intractable size of the matrix is the reason for using iterative methods.

We note that a large number of wavelength points are needed for an accurate evaluation of the radiative flux divergence in equation (4). Each wavelength point needs a solution of a problem equivalent to the integral equation, and it is prohibitive to solve this scattering problem at several hundred wavelength points per time step in simulations. This is the reason for using group mean opacities, which reduce computer time by a factor of typically 100, at the expense of a less accurate solution.

3. METHODS OF SOLUTION

First, we develop the multigroup method, then the iteration scheme; finally, we compare the new iteration method with existing methods.

3.1. *The Multigroup Method*

3.1.1. *Determination of Groups*

We follow the group definition of Nordlund (1982). The atmospheric height range is divided into a chosen number of intervals. A set of wavelengths belong to the same group if the associated monochromatic optical depths are unity within the same height interval. This definition serves to sort wavelength points with similar shapes of the kernel function into the same group. Furthermore, strong lines fall within one group corresponding to high layers, and the continua fall within one group corresponding to deeper layers.

Specifically, the height scale is chosen as a standard optical depth along the vertical direction rather than geometrical height. The standard and monochromatic optical depths can be calculated in the plane-parallel atmosphere of the mean model (horizontally and temporally averaged). The group number i for monochromatic wavelength j is determined by

$$i = \mathrm{Int}\left\{\frac{\log[\tau_0(\tau_j = 1)]}{\Delta \log(\tau)}\right\} + \mathrm{const.} \, ,$$

where "Int" means nearest integer value, $\tau_0(\tau_j = 1)$ is the standard optical depth where the monochromatic optical depth is unity, and $\Delta\log(\tau)$ depends on the number of groups chosen.

We will calculate integrals over wavelength within each group as follows. The set of wavelengths λ_j that belongs to group i is denoted by $\Delta\lambda_i$. This set need not be continuous, since wavelengths in the infrared and ultraviolet can be included in the same group, while a wavelength in the visible can be included in another group. An integration within each group can be carried out also in this case. This is implemented numerically as a quadrature sum:

$$Y_i = \sum_{\Delta\lambda_i} Y_{\lambda_j} w_j \, ,$$

where λ_j and w_j are the wavelength quadrature points and weights, respectively, and Y_{λ_j} an arbitrary wavelength-dependent quantity. In the following, we denote this quadrature sum by the notation of continuous integrals:

$$Y_i = \int_{\Delta\lambda_i} Y_\lambda \, d\lambda \, .$$

3.1.2. *Exact Solution*

Here we derive the exact transport equation for the wavelength-integrated intensity within a wavelength group. The result cannot be used in practice to solve for the wavelength-integrated intensity, since it involves knowledge of the monochromatic radiation field, which we will not solve for. The derivation is made to arrive at approximate solutions that can be used without having knowledge of the

monochromatic radiation field. Integration of the monochromatic transport equation (eq. [3]) over the subset of wavelengths $\Delta\lambda_i$ gives

$$\int_{\Delta\lambda_i} \frac{\partial I_\lambda}{\partial r}\, d\lambda = \int_{\Delta\lambda_i} (\sigma_\lambda J_\lambda + \kappa_\lambda B_\lambda - \chi_\lambda I_\lambda) d\lambda \; .$$

Here we have used equation (1) for the monochromatic emissivity. We use the following notation for the integrated transport equation:

$$\frac{\partial I_i}{\partial r} = \sigma_i^{\rm J} J_i + \kappa_i^{\rm B} B_i - \chi_i^{\rm I} I_i \; . \tag{8}$$

The integrated intensity is

$$I_i = \int_{\Delta\lambda_i} I_\lambda \, d\lambda \; ,$$

the integrated mean intensity is

$$J_i = \int_{\Delta\lambda_i} J_\lambda \, d\lambda = \frac{1}{4\pi} \int_{\Delta\lambda_i} \int_\Omega I_\lambda \, d\Omega \, d\lambda = \frac{1}{4\pi} \int_\Omega I_i \, d\Omega \; ,$$

and the integrated Planck distribution is

$$B_i = \int_{\Delta\lambda_i} B_\lambda \, d\lambda \; .$$

The following definitions satisfy equation (8) for I_i with J_i and B_i in the emissivity term. The group mean scattering opacity is

$$\sigma_i^J = \frac{\int_{\Delta\lambda_i} \sigma_\lambda J_\lambda \, d\lambda}{J_i} \; , \tag{9}$$

which is dependent on the unknown J_λ. The Planck mean absorption opacity is

$$\kappa_i^B = \frac{\int_{\Delta\lambda_i} \kappa_\lambda B_\lambda \, d\lambda}{B_i} \; . \tag{10}$$

The group mean opacity that defines the mean optical path lengths for equation (8) is

$$\chi_i^I = \frac{\int_{\Delta\lambda_i} \chi_\lambda I_\lambda \, d\lambda}{I_i} \; . \tag{11}$$

This opacity is direction dependent because of the direction dependency of I_λ; furthermore, it is dependent on the unknown I_λ.

The group mean source function for this problem follows from the ratio between group mean emissivity and group mean opacity from equation (8). Hence,

$$S_i = \frac{\sigma_i^J J_i + \kappa_i^B B_i}{\chi_i^I} \; .$$

Equation (8) results in a lambda operator for J_i, the kernel of which is a function of χ_i^I only (analogous to eq. [5]), and that acts on S_i:

$$J_i = \Lambda(\chi_i^I)[S_i] \; .$$

3.1.3. *Approximate Solution in the Streaming Regime*

In regions where radiation is nondiffusive (streaming regime), we have to solve the transport equation to account for nonlocal radiation coupling within the gas. The scattering opacity σ_i^J (eq. [9]) and total opacity χ_i^I (eq. [11]) in the exact transport equation (eq. [8]) cannot be precalculated without knowledge of the monochromatic intensity I_λ. Instead, we use the monochromatic radiation field from the same scattering problem from the plane-parallel version of the atmosphere. This is a one-time computation and it is also relatively fast. We get the one dimensional intensity $I_\lambda^{\rm pp}$ and mean intensity $J_\lambda^{\rm pp}$, where "pp" denotes "plane parallel." Both of these quantities are a function of atmospheric height.

As an approximation, we solve equation (8) with scattering opacity and total opacity that are precalculated with this plane-parallel radiation field. We assume that $J_\lambda \simeq J_\lambda^{\rm pp}$ and replace the scattering opacity σ_i^J with the approximate $\sigma_i^{J^{\rm pp}}$:

$$\sigma_i^J \simeq \sigma_i^{J^{\rm pp}} = \frac{\int_{\Delta\lambda_i} \sigma_\lambda J_\lambda^{\rm pp} \, d\lambda}{\int_{\Delta\lambda_i} J_\lambda^{\rm pp} \, d\lambda} \; .$$

Similarly, we could choose to use $I_\lambda^{\rm pp}$ in the calculation of the total opacity. This would, however, introduce a direction dependency. As a first approximation, we eliminate the direction dependency by setting $I_\lambda \simeq J_\lambda^{\rm pp}$ in the averaging, and replace χ_i^I with $\chi_i^{J^{\rm pp}}$:

$$\chi_i^I \simeq \chi_i^{J^{\rm pp}} = \frac{\int_{\Delta\lambda_i} \chi_\lambda J_\lambda^{\rm pp} \, d\lambda}{\int_{\Delta\lambda_i} J_\lambda^{\rm pp} \, d\lambda} \; . \tag{12}$$

Hence, the approximate wavelength averaged intensity I_i^* is defined by the transport equation:

$$\frac{\partial I_i^*}{\partial r} \equiv \sigma_i^{J^{\rm pp}} J_i^* + \kappa_i^B B_i - \chi_i^{J^{\rm pp}} I_i^* \; , \tag{13}$$

where the approximate mean intensity is

$$J_i^* = \frac{1}{4\pi} \int_\Omega I_i^* \, d\Omega \; .$$

The ratio between emissivity and opacity gives the source function

$$S_i^* = \frac{\sigma_i^{J^{\rm pp}} J_i^* + \kappa_i^B B_i}{\chi_i^{J^{\rm pp}}} \; . \tag{14}$$

The Planck mean absorption opacity in equation (10) remains unchanged, since the Planck distribution is always defined for a given temperature. Hence, the thermal emissivity $\kappa_i^B B_i$ has remained exact. Since equation (13) has the standard transport equation format, we get a lambda operator kernel that is a function of $\chi_i^{J^{\rm pp}}$ and that acts on the source function S_i^*:

$$J_i^* = \Lambda(\chi_i^{J^{\rm pp}})[S_i^*] \; . \tag{15}$$

The largest inaccuracies in the approach given above result from using $J_\lambda^{\rm pp}$ as a weight function in the averaging of the total opacity (eq. [12]), since the correct weight function I_λ is strongly direction dependent.

3.1.4. *Approximate Solution in the Diffusion Limit*

The diffusion limit is characterized by small photon mean free paths (high opacity) compared to the scale of variation of the source function. In this case, the lambda operator is local because of the rapid cutoff of the kernel function by the exponential dependency of the optical path length (eq. [5]). Hence, $J_\lambda \simeq S_\lambda$. This implies $S_\lambda \simeq B_\lambda$ by equation (2),

even if scattering is dominating. The solution of the transport equation (eq. [3]) is in this case to first order (e.g., Mihalas 1978):

$$I_\lambda = B_\lambda - \frac{1}{\chi_\lambda}\frac{\partial B_\lambda}{\partial r} .$$

The wavelength averaged intensity becomes

$$I_i = B_i - \frac{1}{\chi_i^R}\frac{\partial B_i}{\partial r} , \tag{16}$$

where χ_i^R is the *Rosseland group mean opacity* defined by

$$\frac{1}{\chi_i^R} = \int_{\Delta\lambda_i} \frac{1}{\chi_\lambda}\frac{\partial B_\lambda}{\partial r}\, d\lambda \Big/ \int_{\Delta\lambda_i} \frac{\partial B_\lambda}{\partial r}\, d\lambda .$$

We want to use a form of the transport equation in both streaming and diffusion limits such that both limits will be satisfied in a global numerical solution. The alternative would be to split the numerical scheme and compute the Rosseland flux divergence directly by using three-dimensional gradient operators in diffusive layers and use the transport equation in the streaming limit in atmospheric layers. The transport equation that satisfies equation (16) in the diffusion limit results from using χ_i^R as the total opacity:

$$\frac{1}{\chi_i^R}\frac{\partial I_i^*}{\partial r} = S_i^* - I_i^* , \tag{17}$$

where we must assure that $S_i^* \to B_i$. Again,

$$J_i^* = \Lambda(\chi_i^R)[S_i^*] . \tag{18}$$

For small mean free paths, we have $J_i^* \simeq S_i^*$.

The correct weight used in the source function for the scattering and total opacities is now the Planck distribution since the mean intensity approaches the Planck distribution in the limit. This also gives the correct three-dimensional variations, which the plane-parallel mean intensity cannot account for. Hence, equation (14) is rewritten as

$$S_i^* = \frac{\sigma_i^B J_i^* + \kappa_i^B B_i}{\chi_i^B} , \tag{19}$$

where the group mean scattering opacity is given by

$$\sigma_i^B = \frac{\int_{\Delta\lambda_i} \sigma_\lambda B_\lambda\, d\lambda}{B_i} , \tag{20}$$

and the Planck mean opacity by

$$\chi_i^B = \frac{\int_{\Delta\lambda_i} \chi_\lambda B_\lambda\, d\lambda}{B_i} . \tag{21}$$

As $J_i^* \to S_i^*$, this source function satisfies the requirement $S_i^* \to B_i$. It also satisfies $S_i^* = B_i$ for pure absorption where $\kappa_i^B = \chi_i^B$, and $S_i^* = J_i^*$ for pure scattering where $\sigma_i^B = \chi_i^B$.

3.1.5. *Weighting between Diffusion and Streaming Regimes*

The source function for the streaming limit in equation (14) and for the diffusion limit in equation (19) is combined into one source function using a weighting function between the two limits:

$$S_i^* = \left(\frac{\sigma_i^{J\text{pp}} \to \sigma_i^B}{\chi_i^{J\text{pp}} \to \chi_i^B}\right) J_i^* + \frac{\kappa_i^B B_i}{\chi_i^{J\text{pp}} \to \chi_i^B} \equiv \rho_i J_i^* + \eta_i , \tag{22}$$

where we have defined a group mean scattering albedo ρ_i and a group mean thermal source η_i. The arrows indicate transition to the diffusion limit in optically thick layers. We use the same weighting function for the group mean opacities used in the lambda operators in equations (15) and (18):

$$\chi_i^{J\text{pp}} \to \chi_i^R \equiv \chi_i^T , \tag{23}$$

where we have defined the combined group mean opacity χ_i^T. The mean intensity for both regimes is given by

$$J_i^* = \Lambda(\chi_i^T)[S_i^*] ,$$

or in terms of the transport equation,

$$\frac{\partial I_i^*}{\partial r} = \chi_i^T (S_i^* - I_i^*) . \tag{24}$$

What remains to define is the weighting function. We treat the radiation problem as nondiffusive within a group when the Rosseland photon mean free path $l_i^{\text{mfp}} = 1/\chi_i^R$ is larger than a typical length scale of variation l_i of the group mean Planck function. This weighting is three dimensional since the Rosseland group mean opacity varies from grid point to grid point. We choose the "optically thin weight" by the exponential

$$W_{\text{stream}} = \exp(-l_i \chi_i^R) .$$

For weighting between streaming regime opacities X_{stream} and diffusion regime opacities X_{diffuse} in both source function and transport equation, we use

$$X = W_{\text{stream}} X_{\text{stream}} + (1 - W_{\text{stream}}) X_{\text{diffuse}} , \tag{25}$$

which in our arrow notation is

$$X = X_{\text{stream}} \to X_{\text{diffuse}} .$$

3.1.6. *Consistency in the Monochromatic Limit*

We recover the exact monochromatic solution if the wavelength interval of a group approaches zero. In this limit, the form of the weighting functions in the opacity averages plays no role, and the source function in equation (22) becomes the monochromatic source function in equation (2). The opacity used in the transfer equation, equation (23), becomes the monochromatic opacity. The form of depth weighting plays no role in this case, since the transition is made between two identical quantities.

3.1.7. *Approximate Flux Divergence*

The exact wavelength-integrated flux divergence is for each group:

$$\nabla \cdot \boldsymbol{F}_i = \int_\Omega \int_{\Delta\lambda_i} \frac{\partial I_\lambda}{\partial r}\, d\lambda\, d\Omega = \int_\Omega \frac{\partial I_i}{\partial r}\, d\Omega . \tag{26}$$

For the approximate I_i^* from equation (24), we get the flux divergence

$$\nabla \cdot \boldsymbol{F}_i^* = \int_\Omega \frac{\partial I_i^*}{\partial r}\, d\Omega = \int_\Omega \chi_i^T (S_i^* - I_i^*) d\Omega . \tag{27}$$

This becomes in the streaming limit, using equations (14) and (13),

$$\int_\Omega \chi_i^{J\text{pp}} (S_i^* - I_i^*) d\Omega = 4\pi(\kappa_i^B B_i - \kappa_i^{J\text{pp}} J_i^*) ,$$

where $\kappa_i^{J\text{pp}} = \chi_i^{J\text{pp}} - \sigma_i^{J\text{pp}}$ is the group mean absorption opacity. We note that the approximation lies in the absorption term $\kappa_i^{J\text{pp}} J_i^*$ and that the thermal emission term $\kappa_i^B B_i$ is

exact. The approximate flux divergence in the diffusion limit becomes, when using equations (16), (17), and the source function in equation (19) in the limit $S_i^* \to B_i$:

$$\int_\Omega \chi_i^R (B_i - I_i^*) d\Omega = -\int_\Omega \frac{\partial}{\partial r} \frac{1}{\chi_i^R} \frac{\partial B_i}{\partial r} \, d\Omega \, .$$

The total exact flux divergence is obtained by summation over all groups according to equations (4) and (26):

$$\nabla \cdot \boldsymbol{F} = \sum_i \nabla \cdot \boldsymbol{F}_i = \int_\Omega \int_0^\infty \frac{\partial I_\lambda}{\partial r} \, d\lambda \, d\Omega \, ,$$

and, similarly, we have that the total approximate flux divergence is

$$\nabla \cdot \boldsymbol{F}^* = \sum_i \nabla \cdot \boldsymbol{F}_i^* \, . \tag{28}$$

3.2. *The Iteration Scheme*

3.2.1. *Notation Definition*

Here, we derive the iteration method to solve for either the monochromatic radiation or for the radiation in individual groups. Both problems have the same form for the transport equation and, therefore, we will use a general formalism in this section. The general transport equation is

$$\pm \frac{1}{\chi} \frac{\partial I^\pm}{\partial r} = S - I^\pm \, , \tag{29}$$

where χ is χ_i^T for groups, and χ_λ for the monochromatic problem. $I^\pm$ is the intensity in the two opposite directions along a given ray. This ray has an arbitrary direction, and r is the geometrical distance along this ray from an arbitrary point. I^+ is chosen to be in the direction of increasing distance r and I^- in the direction of decreasing r. The source function S is given by equation (22) for groups and by equation (2) for the monochromatic problem. In both cases, we write S in terms of a scattering albedo ρ, mean intensity J, and thermal source η:

$$S = \rho J + \eta \, . \tag{30}$$

The iterative method uses the bidirectional average intensity as the unknown variable:

$$p_\Omega = \tfrac{1}{2}(I^+ + I^-) \, ,$$

where Ω denotes the direction dependency. The transfer equations for I^+ and I^- (eq. [29]) can be recast to the familiar second-order differential equation first formulated by Feautrier (1964):

$$\left(1 - \frac{\partial^2}{\partial \tau_\Omega^2}\right) p_\Omega = S \, . \tag{31}$$

τ_Ω is the optical path length along the associated ray, and the relation to opacity and geometrical distance is

$$d\tau_\Omega = \chi \, dr \, .$$

We define the inverse lambda operator for a single ray as

$$\Lambda_\Omega^{-1} \equiv 1 - \frac{\partial^2}{\partial \tau_\Omega^2} \, . \tag{32}$$

Hence, p_Ω can be written in terms of the lambda operator for a single ray:

$$p_\Omega = \Lambda_\Omega[S] \, .$$

The explicit form of this operator follows from using the integrated transport equation (eq. [29]) for I^+ and I^-:

$$\Lambda_\Omega[S] = \tfrac{1}{2}\left(\int_0^\infty S \exp(-\tau_\Omega^+) d\tau_\Omega^+ + \int_0^\infty S \exp(-\tau_\Omega^-) d\tau_\Omega^- \right) , \tag{33}$$

where τ_Ω^+ and τ_Ω^- are the optical lengths measured along opposite directions for a given ray. The integrations are started from the point where p_Ω is evaluated (where $\tau_\Omega^+ = \tau_\Omega^- = 0$). Note that p_Ω can be found in two ways for a given source function; either by solving the differential equation $\Lambda_\Omega^{-1}[p_\Omega] = S$, or by integrating over the source function directly, using $p_\Omega = \Lambda_\Omega[S]$. The mean intensity is given by

$$J = \int_\Omega p_\Omega \frac{d\Omega}{2\pi} \, . \tag{34}$$

Hence, the full lambda operator is formally given by the relations

$$J = \Lambda[S] = \int_\Omega \Lambda_\Omega[S] \frac{d\Omega}{2\pi} \, . \tag{35}$$

The integration is done over a half-sphere (spanning the solid angle 2π). By combining equations (34), (32), and (31) with equation (30), we get the integrodifferential equation for p_Ω that specifies our problem:

$$\Lambda_\Omega^{-1}[p_\Omega] = \rho \int_\Omega p_\Omega \frac{d\Omega}{2\pi} + \eta \, . \tag{36}$$

Alternatively, we can formulate the problem as an integral equation in the source function by combining equation (35) with equation (30):

$$S = \rho \Lambda[S] + \eta \, . \tag{37}$$

We use the integrodifferential form in the derivation of the iteration method.

3.2.2. *Iterations with Ray Decoupling*

With the formalism given above, we are in a position to derive the iteration method. Let p_Ω^n be the current estimate of the unknown p_Ω at iteration step n. The corresponding estimate of the source function is, by using equations (30) and (34):

$$S^n = \rho \int_\Omega p_\Omega^n \frac{d\Omega}{2\pi} + \eta \, . \tag{38}$$

The corresponding formal solution is given by

$$p_\Omega^{\rm FS} = \Lambda_\Omega[S^n] \, , \tag{39}$$

and let $S^{\rm FS}$ be given by

$$S^{\rm FS} = \rho \int_\Omega p_\Omega^{\rm FS} \frac{d\Omega}{2\pi} + \eta \, , \tag{40}$$

which is equivalent to $S^{\rm FS} = \rho \Lambda[S^n] + \eta$. Since the solution S satisfies equation (37), we have that both $S^{\rm FS}$ and S^n approach S for a convergent iteration. Hence, we must also have that $S^{\rm FS} \to S^n$. We therefore define an error in the source function by

$$E^n = S^{\rm FS} - S^n \, . \tag{41}$$

This error term is used for calculating approximate corrections to the radiation field, and these corrections approach

zero when the error term approaches zero. We rewrite the error by using the inverted version of equation (39) for S^n and equation (40) for S^{FS}:

$$E^n = \rho \int_\Omega p_\Omega^{FS} \frac{d\Omega}{2\pi} + \eta - \Lambda_\Omega^{-1}[p_\Omega^{FS}] . \quad (42)$$

The exact correction $\delta p_\Omega = p_\Omega - p_\Omega^{FS}$ is added to p_Ω^{FS} in this equation, which by equation (36) results in $E^n = 0$. This can be written as

$$\rho \int_\Omega (p_\Omega^{FS} + \delta p_\Omega) \frac{d\Omega}{2\pi} + \eta - \Lambda_\Omega^{-1}[p_\Omega^{FS} + \delta p_\Omega] = 0 . \quad (43)$$

Subtraction of equation (42) from equation (43), and using the fact that Λ_Ω^{-1} is linear since we have assumed that the opacity χ is independent of the radiation field, yields an equation for the exact correction δp_Ω:

$$\Lambda_\Omega^{-1}[\delta p_\Omega] - \rho \int_\Omega \delta p_\Omega \frac{d\Omega}{2\pi} = E^n . \quad (44)$$

The angle integral results in a coupled set of second-order differential equations as for the original problem in equation (36) and is equally difficult to solve. We therefore make a simplification in the angle integral, and the solution of the equation will now define approximate instead of exact corrections. This leads to an iteration series that we must provide convergence for. The accuracy of the simplified angle integral determines the convergence rate. The error term E^n includes S^{FS}, which is calculated using the full angle integral in equation (40), such that S^n will converge to the correct solution.

We assume that the corrections δp_ω in an arbitrary direction ω in a subset of ray directions $\Delta\Omega_c$ are comparable to the angle averaged correction:

$$\delta p_\omega \sim \int_\Omega \delta p_\Omega \frac{d\Omega}{2\pi} = \delta J ; \quad \omega \in \Delta\Omega_c . \quad (45)$$

Since any direction $\omega \in \Delta\Omega_c$ gives approximately the same correction by this assumption, it is only necessary to solve for the approximate correction without coupling to other rays in $\Delta\Omega_c$. The equation for the corrections is defined by inserting equation (45) in equation (44):

$$\Lambda_\omega^{-1}[\delta p_\omega^*] - \rho \, \delta p_\omega^* \equiv E^n . \quad (46)$$

This approach is exact in the special case of optically thick media, for which any direction gives the same perturbation because of isotropy. In optically thin three-dimensional media, the solutions from equation (46) will be slightly different for different ω. We therefore solve the equation on several rays in $\Delta\Omega_c$, and the angle average of these perturbations gives a more accurate estimate of the perturbation in mean intensity:

$$\delta J^* = \frac{1}{\Delta\Omega_c} \int_{\Delta\Omega_c} \delta p_\omega^* \, d\omega \simeq \int_\Omega \delta p_\Omega \frac{d\Omega}{2\pi} = \delta J . \quad (47)$$

For the special case of planetary or stellar atmospheres, which have roughly a plane-parallel character, we could use a one-point angular quadrature in zenith angle (Eddington approximation for plane-parallel atmospheres) and choose a set of points in azimuth angle to define $\Delta\Omega_c$. This corresponds to a bidirectional cone symmetrical about the vertical line.

The approximate perturbation in mean intensity δJ^* is now used to find the next estimate of the source function S^{n+1}. Equation (43) for the exact correction can be rewritten as

$$S^{FS} + \rho \, \delta J - S = 0 .$$

Hence, the next estimate S^{n+1} of S becomes

$$S^{n+1} = S^{FS} + \rho \, \delta J^* = S^{FS} + \delta S^* . \quad (48)$$

The iteration steps can be summarized as follows (using the left-hand side results on the right-hand side in the following line):

$$S^{FS} = \rho\Lambda[S^n] + \eta$$
$$E^n = S^{FS} - S^n$$
$$\Lambda_\omega^{-1}[\delta p_\omega^*] - \rho \, \delta p_\omega^* = E^n$$
$$\delta J^* = \frac{1}{\Delta\Omega_c} \int_{\Delta\Omega_c} \delta p_\omega^* \, d\omega$$
$$S^{n+1} = S^{FS} + \rho \, \delta J^* .$$

3.3. *Comparison with Other Three-Dimensional Iterative Methods*

It is now instructive to discuss other methods and to compare them with the present method. It will then become clear that the present method is favorable for the coherent isotropic scattering problem.

3.3.1. *Cannon's AQPT Method*

The Angle Quadrature Perturbation Technique (AQPT) of Cannon (1973a) is related to the present method in that the angle integral is approximated and that the integrodifferential approach is used as a basis. The angle integral for the corrections is represented by a quadrature sum with fewer angles (lower order quadrature) than the more accurate quadrature sum used for the formal solution of the mean intensity needed in the error term. All rays in the lower order quadrature sum are used in the correction procedure, and this corresponds to a set of coupled differential equations. This is computationally demanding in three-dimensions since it leads to a matrix equation with a complex matrix structure.

Cannon's method results if, instead of the one-ray approximation in equation (45), we use an approximate angle integral with few quadrature points Ω_i. This replaces the angle integral[2] in equation (44):

$$\Lambda_{\Omega_i}^{-1}[\delta p_{\Omega_i}^*] - \rho \sum_i \delta p_{\Omega_i}^* w_i = E^n . \quad (49)$$

Here, w_i are the quadrature weights. All perturbations $\delta p_{\Omega_i}^*$ are found simultaneously instead of finding them successively, ray by ray. The perturbation in mean intensity is given by

$$\delta J^* = \sum_i \delta p_{\Omega_i}^* w_i . \quad (50)$$

As a special case of Cannon's method, we can use only one ray Ω_0 in the approximate angle integral that gives the one-ray approximation we have used. However, this corre-

[2] The symbols of continuous integrals means that they are implemented numerically as high-order quadrature sums. The approximate angle integral is written explicitly as a quadrature sum to distinguish it from the more accurate angle integral.

sponds to $\delta J^* = \delta p^*_{\Omega_0}$ by equation (50) and is not the same as the present method, since we average over several solutions of the correction equation (eq. [46]) to get the corrections in mean intensity.

3.3.2. *Local ALI Method*

Equation (37) for the volume integral form of the problem has been solved by iterations using the well-known Accelerated Lambda Iteration technique (ALI) (e.g., Hubeny 1992). For three-dimensional problems, it is most convenient to use the diagonal (local) elements Λ_{ii} of the kernel matrix as the approximate operator since this involves only scalar operations, grid point by grid point, for the corrections to the source function. This scheme is, in our case, identical to Jacobi iterations (Jacobi 1845). In practice, one uses the approximate diagonal elements Λ^*_{ii} (e.g., Olson, Auer, & Buchler 1986). The correction to the source function is now

$$\delta S^* = \frac{E^n}{1 - \rho\Lambda^*_{ii}} .$$

The updated value is $S^{n+1} = \delta S^* + S^n$.

3.3.3. *Discussion of Methods*

The ALI method is characterized by approximations in spatial coupling and accurate angle coupling while Cannon's and the present method are characterized by approximations in angle coupling and accurate spatial coupling.

The ALI method has a much slower convergence rate than the present method (as shown by Botnen 1997) since it does not provide global coupling along rays. The time spent on formal solutions for the error term will therefore be larger because there are more iteration steps. Cannon's method involves coupled differential equations through the approximate angle integral and results in intractable matrix equations in practice when the problem is three dimensional.

The correction step in the current method provides a faster convergence rate than ALI while avoiding the coupled rays as in Cannons's method. Equation (46) for the corrections can be written as

$$W[\delta p^*_\omega] \equiv (\Lambda_\omega^{-1} - \rho)[\delta p^*_\omega] = E^n . \tag{51}$$

Hence, W can be written as a matrix by subtracting ρ from the diagonal elements in the standard Feautrier matrix. The Feautrier matrix is tridiagonal, and this results from using finite differences for the second derivative in the Λ_Ω^{-1} operator (eq. [32]). The matrix form of W is therefore also tridiagonal and the solution of $W[\delta p^*_\omega] = E^n$ requires only on the order of D arithmetic operations, where D is the number of points along a ray. Hence, the correction procedure is relatively cheap computationally.

4. APPLICATION TO SOLAR SIMULATIONS

We have extended the solar convection model of Nordlund & Stein (1990) to include chromospheric layers. Radiation was previously treated in LTE by using averaged Planck functions in a few wavelength groups as source functions, according to the procedure explained in Nordlund (1982). The new model extends to 1.5 Mm above the granular layer (as compared with 500 km in the previous model). The lower boundary is located 1.5 Mm below the top of the convection zone. This gives a total vertical extension of 3 Mm. We solve the radiation scattering problem from the top of the domain down to a layer within the convective part of the simulation. This zone covers about 10 orders of magnitude in opacity.

For each time step and wavelength group, we start the iteration with the solution from the previous time step. After convergence of all groups, we calculate the radiative flux divergence and add that to the gas-energy equation. Hydrodynamic results from these simulations are treated elsewhere (Skartlien 1998; Skartlien et al. 2000).

In this section, we explain the numerical implementation, discuss the performance of the iteration scheme, and the treatment of opacities.

4.1. *Numerical Implementation*

4.1.1. *Radiation Boundary Conditions*

We use incoming intensities at the upper and lower boundaries of the domain as the two boundary conditions in Feautrier's scheme. We assume a constant source function above the upper boundary, and the incoming intensity is calculated accordingly. The incoming intensity at the lower boundary is calculated using the diffusion approximation as in equation (16). The horizontal boundaries are periodic, such that outgoing, slanted rays at one sidewall enter the domain at the opposite sidewall. This makes it possible to always use rays that extend from the top to the bottom boundaries and to use only these boundary conditions.

4.1.2. *Ray Discretization*

We use Cartesian coordinates (orthogonal coordinate axes), which is suitable for a sufficiently small domain where the solar/stellar curvature can be neglected. The long characteristics method is used for the radiation, with sampling only on horizontal planes (Nordlund 1985), such that every ray consists of the N_z depth points. This results in relatively simple algorithms suitable for parallel processing, since there are no computational differences for varying ray direction.

It is noted that the short characteristics (SC) method (Kunasz & Auer 1988) has better resolution along slanted rays since vertical planes also are sampled. We cannot use the SC method within the present ray-based correction procedure.

For the high-resolution angle integral over $p^{\rm FS}_\Omega$ (for $S^{\rm FS}$ in the error term E^n), we use Gaussian quadrature integration over zenith angle and trapezoidal integration with even spacing over azimuthal angle. This choice corresponds to rays along a set of bidirectional cones centered on the vertical line. All rays in the cone with smallest zenith angle defines our subset of angles in which we solve the correction equation. This choice gives a faster convergence rate than using rays with larger angles from the vertical line.

4.1.3. *Interpolation between Rays and Cartesian Grid*

We have $N_x \times N_y$ parallel rays passing through each horizontal plane for each ray direction. (N_x and N_y are the number of grid points in the horizontal directions). These rays do not necessarily pass through grid points, and we must therefore interpolate values from grid points onto rays. We also need to do the reverse interpolation from rays to grid. We use a local spline interpolation procedure as in Nordlund (1982).

These interpolations are not reversible, as opposed to the Fourier interpolations used in Nordlund (1985) and Kisel-

man & Nordlund (1995). The aliased components in the discrete Fourier transform are sufficient to introduce an instability in the iteration procedure. This could be the reason why Kiselman & Nordlund (1995) applied a stabilizing "extra" lambda iteration in their scheme. The high spatial frequencies are successively amplified if a lowpass (de-aliasing) filter is not applied.

We have therefore used a more robust spline interpolation. This need not be reversible as long as we avoid interpolating the same quantity back and forth between the grid and rays during the iteration. This situation arises in the deepest layers where the specific intensity is equal to the source function. The next estimate of the source function should in this case be equal to the previous estimate and the error term would be zero. However, this is not exactly true for nonreversible interpolations. We solve this problem by solving for the difference $q_\Omega^{\rm FS} = p_\Omega^{\rm FS} - S^n$ in optically thick layers. This approach ensures a zero error term where $q^{\rm FS}$ vanishes, independently from the choice of interpolation scheme. The differential equation for $q^{\rm FS}$ is obtained by taking the second derivative in optical path length τ_Ω of equation (31):

$$\Lambda_\Omega^{-1}[q_\Omega^{\rm FS}] = \frac{\partial^2 S^n}{\partial \tau_\Omega^2} . \tag{52}$$

4.1.4. *Implementation of Iterations*

Let "g" be grid variables and "r" ray variables, and let arrows denote interpolations between grid and rays. We suppress the angular index Ω of $p^{\rm FS}$ and $q^{\rm FS}$ for clarity. We use logarithmic interpolation for quantities that are always positive (such as intensity) to avoid unphysical negative interpolants.

For a given S_g^n, we calculate the error E_g^n by the following procedure:

$$\log(\chi_g) \rightarrow \log(\chi_r)$$
$$\log(S_g^n) \rightarrow \log(S_r^n) .$$

After the solution of equation (31) for optically thin layers:

$$\log(p_g^{\rm FS}) \leftarrow \log(p_r^{\rm FS}) .$$

After the solution of equation (52) in optically thick layers:

$$q_g^{\rm FS} \leftarrow q_r^{\rm FS} .$$

We calculate the formal solution $S_g^{\rm FS}$ by running through all ray directions by repeated usage of the last four equations. For optically thick layers:

$$S_g^{\rm FS} = \rho_g \left(\sum_\Omega q_g^{\rm FS} w_\Omega + S_g^n \right) + \eta_g .$$

For optically thin layers:

$$S_g^{\rm FS} = \rho_g \sum_\Omega p_g^{\rm FS} w_\Omega + \eta_g .$$

The error is now calculated (eq. [41]) as

$$E_g^n = S_g^{\rm FS} - S_g^n .$$

We can now calculate the correction to the source function δS_g^*. These interpolations are done for the corrector step

$$\log(\chi_g) \rightarrow \log(\chi_r)$$
$$E_g^n \rightarrow E_r^n .$$

We have that $\epsilon_g = 1 - \rho_g$, where ρ_g is the scattering albedo and ϵ_g the destruction probability. Since $\epsilon_g \in [0,1]$, we must ensure that the same is true for the interpolant. To do this, we use these transformations:

$$a_g = \frac{\epsilon_g}{1 - \epsilon_g}$$
$$\log(a_g) \rightarrow \log(a_r)$$
$$\epsilon_r = \frac{a_r}{1 + a_r} \in [0, 1] .$$

The corrections δp_r^* are now calculated from equation (46). Then we interpolate these corrections back to the grid:

$$\delta p_g^* \leftarrow \delta p_r^* .$$

δS_g^* is calculated by using the last six equations while running through the subset of angles. The quadrature sum over the subset of angles gives

$$\delta S_g^* = \rho_g \sum_\omega \delta p_g^* w_\omega .$$

w_ω are the angle quadrature weights. The updated source function is by equation (48):

$$S_g^{n+1} = S_g^{\rm FS} + \delta S_g^* .$$

We can now go back to the calculation of the error term for the next iteration.

After convergence of this scheme, we calculate the flux divergence contributions along each ray and interpolate these back to the grid:

$$\left\{ \frac{\Delta\tau_\Omega}{\Delta r} (S - p_\Omega) \right\}_g \leftarrow \left\{ \frac{\Delta\tau_\Omega}{\Delta r} (S - p_\Omega) \right\}_r .$$

The flux divergence per group is obtained by the angle integration in equation (27). The total flux divergence is obtained by adding over all groups according to equation (28):

$$\nabla \cdot \boldsymbol{F}^* = \sum_i \sum_\Omega \left\{ \frac{\Delta\tau_\Omega}{\Delta r} (S - p_\Omega) \right\}_g w_\Omega .$$

4.2. *Performance in Simulations*

4.2.1. *CPU Time as Function of Resolution*

The CPU time spent on spline interpolations per ray direction scales linearly with $N_{\rm grid} = N_x N_y N_z$. This is also the case for the formal solutions $p_\Omega^{\rm FS}$ along rays, since there are $N_x N_y$ rays per direction, and the solution of $p_\Omega^{\rm FS}$ per ray scales as N_z. The CPU time for the formal solution $S^{\rm FS}$ is therefore

$$T_{\rm FS} = a N_{\rm rays} N_{\rm grid} ,$$

where a is a constant. $N_{\rm rays}$ denotes the number of ray directions. Here, we have not taken into account external arithmetical operations since they consume a negligible amount of time in comparison. Similarly, the time spent on corrections δS^* is

$$T_{\rm corr} = b(\alpha N_{\rm rays}) N_{\rm grid} ,$$

where $b \simeq a$ is a constant, and $\alpha = N_{\rm subset}/N_{\rm rays} < 1$, and where $N_{\rm subset}$ is the number of rays in the correction pro-

cedure. $\alpha = 1/3$ when using one set of azimuthal angles from three sets defined by a three-point Gaussian quadrature in zenith angle. The CPU-time for one iteration step in one wavelength group is $T_{\rm it} = T_{\rm FS} + T_{\rm corr}$. Hence, the total CPU time for solving for the radiation also scales linearly with the number of ray directions and grid points: $T_{\rm tot} = T_{\rm it} N_{\rm iter} \sim N_{\rm rays} N_{\rm grid} N_{\rm iter}$, where $N_{\rm iter}$ is the total number of iterations needed for all groups. Since $b \simeq a$ and $\alpha < 1$, most of the CPU time is used on formal solutions.

4.2.2. *Parallel Processing*

We have used MPI (Message Passing Interface) on a CRAY ORIGIN 2000 machine to compute formal solutions $p_\Omega^{\rm FS}$ and corrections δp_Ω^* for different angles in parallel (for angle parallelization in combination with the SC method, see Botnen 1997). For each iteration, the data needed for different angles are distributed to the set of microprocessors we use. The resulting ray data are thereafter gathered and averaged (angle integrals) in one microprocessor. This scheme is repeated until convergence of the iteration.

In principle, the *computational time* (not CPU time) will be reduced by a factor $1/N_{\rm rays}$ and $1/N_{\rm subset}$ for formal solutions and corrections, respectively, if we use $N_{\rm rays}$ and $N_{\rm subset}$ microprocessors for formal solutions and corrections. In practice, the time reduction is less because of the transfer of data between microprocessors; more microprocessors means more time for exchanging data. In some cases, we therefore calculate, in succession, results for more than one ray direction per microprocessor. In these cases, the number of microprocessors is less than $N_{\rm rays}$ and $N_{\rm subset}$. A further speed-up would result if we parallelized over groups in addition to ray directions.

4.2.3. *Iteration Convergence*

At each time step in a simulation, and for each group, the source function is iterated to convergence. The initial estimate for the source function $S^{n=0}$ is taken as the converged source function from the previous time step. Orthomin acceleration is used (Vinsome 1976) to improve the convergence rate of the iteration. It is found that Orthomin acceleration (of order 2) reduces the number of iteration steps by a factor of about 2.

The iteration is terminated when the maximum relative change

$$\mathrm{Max}\left[\frac{|S^n - S^{n-1}|}{S^{n-1}}\right]$$

is smaller than a specified limit, typically 10^{-3} (n is iteration number). This corresponds to typically 2, 5, 10, and 15 iterations for groups 1, 2, 3, and 4, respectively. Increasing group number corresponds to smaller destruction probabilities in the atmosphere (see Fig. 2); hence, more iterations are needed.

Figure 1 shows the maximum relative error or deviation from the converged source function S^∞,

$$\mathrm{Max}\left[\frac{|S^n - S^\infty|}{S^\infty}\right],$$

as function of iteration number. We have chosen an arbitrary time step in the simulation and use the converged source function from the previous time step as an initial estimate. In the figure, we see that the typical number of iterations given above (corresponding to 10^{-3} relative changes) correspond to errors of about 5×10^{-3}. Note that

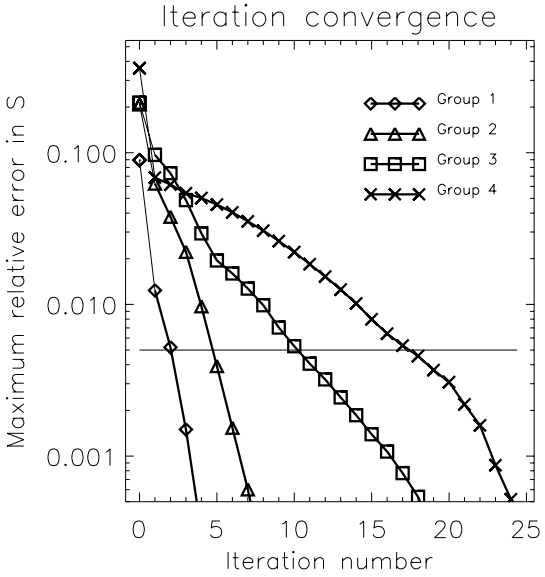

FIG. 1.—Source function convergence for the iteration method, at an arbitrary time step in a solar simulation. Maximum relative errors from the converged source functions are plotted as a function of iteration number. The initial source functions are taken from the previous time step. A relative error of 5×10^{-3} is marked by the line. This corresponds to 2, 5, 10, and 17 iterations. These numbers are typical for the amount of iterations needed in simulations, in which we choose a convergence limit based on relative changes as the source function (typically 10^{-3}) between iterations. More iterations are needed for increasing group number, since the destruction probability (in the atmosphere) is smaller for increasing group number. The convergence curves in this log-plot are roughly linear, corresponding to an exponentially decreasing error with iteration number.

we choose a limit on the maximum relative change as a convergence criterion in simulations since the fully converged source function is not calculated. Figure 1 shows that the errors decrease roughly exponentially with iteration number.

Errors at iteration number 0 show the maximum deviations between the converged source functions at current and previous time steps. We see that these can be as large as 0.3–0.4 (group 4), even if the intervals between time steps are only on the order of 0.1 s of solar time. Iteration of the source function at every time step is therefore needed.

4.3. *Calculation of Group Mean Opacities*

4.3.1. *Monochromatic Continuum and Line Opacities*

Continuum opacities are calculated using the package of Gustafsson (1973). Absorption opacities κ_λ^c are calculated for bound-free and free-free transitions of H^- and H I, for bound-free transitions of H_2^-, H_2, H_2^+, He I, C I, Mg I, Al I, and Si I. Scattering opacities σ_λ^c are calculated for Rayleigh and electron scattering. Electrons come from ionized stages of the most abundant elements H, He, C, N, O, Ne, Na, Mg, Al, Si, S, K, Ca, Cr, Fe, and Ni.

Line opacities χ_λ^l (sum of absorption opacities κ_λ^l and scattering opacities σ_λ^l) for CO and CN molecules and for the strongest lines of the most abundant elements are taken from opacity distribution functions by Gustafsson et. al. (1975). The opacity spectrum consists of 368 wavelength points from 153.3 nm in the ultraviolet to 12.43 μm in the infrared. Line opacities χ_λ^l from Fe in ultraviolet are accounted for by refining the empirical fit of Magain (1983).

4.3.2. *Line Destruction Probability*

The contributions to line opacity from absorption are calculated using the approximation of Van Regemorter (1962). The destruction probability in lines ϵ_λ^l is in general dependent on several electronic transitions k on the same wavelength with individual destruction probabilities $\epsilon_\lambda^{l,k}$:

$$\epsilon_\lambda^l = \frac{\sum_k \chi_\lambda^{l,k} \epsilon_\lambda^{l,k}}{\chi_\lambda^l} = \frac{\kappa_\lambda^l}{\chi_\lambda^l}, \tag{53}$$

where

$$\chi_\lambda^l = \sum_k \chi_\lambda^{l,k}$$

is the total line opacity, and $\chi_\lambda^{l,k}$ the line opacity at a transition k. Hence, this weighting procedure favors those transitions with the largest probability to interact with photons. The destruction probability in transition k is given by the probability for collisional deexcitation from the upper level j to the lower level i:

$$\epsilon_\lambda^{l,k} = \frac{1}{(A_{ji}/C_{ji}) + 1}.$$

A_{ji} [s^{-1}] is the Einstein coefficient for spontaneous radiative deexcitation, and C_{ji} [s^{-1}] is the collisional deexcitation parameter.

We use Van Regemorter's approximation for C_{ji}/A_{ji} that is independent of the specific transition:

$$\frac{C_{ji}}{A_{ji}} = 20.6\lambda^3 n_e T^{-1/2} P_{N,I}\left(\frac{\Delta E}{kT}\right), \tag{54}$$

where λ [cm] is the photon wavelength, n_e [cm^{-3}] electron number density, T [K] temperature, ΔE [ergs] the photon energy, k [ergs K^{-1}] the Boltzmann constant. The function P is given either for positive ions or neutrals.

We use the estimate for line destruction probability $\epsilon_\lambda^l(n_e, T)$ to calculate line-absorption opacities κ_λ^l from equation (53). Line opacities χ_λ^l are taken from opacity distribution functions and from an approximation of the opacity in the ultraviolet caused by numerous iron lines (Magain 1983).

5. TEST OF THE METHODS

5.1. *Monochromatic versus Approximate Solutions*

We compare the total radiative heating ϕ_i^* (negative of flux divergence) in each group with the exact solutions ϕ_i obtained from wavelength integration of monochromatic solutions. The monochromatic solutions are obtained from solving a three-dimensional scattering problem at each of the 368 wavelength points we use. For this test, we have used a single snapshot from the three-dimensional atmosphere-convection simulation, with the current radiation method included in the energy equation.

We use four groups, denoted by 1, 2, 3, and 4, with group 1 as the continuum group and group 4 for the strongest spectral lines. Intermediate groups correspond to weaker lines. Optical depths unity, corresponding to the group mean opacities, are located at increasing height for increasing group number because of larger average opacity for the spectral line groups. Group 1 transports the most radiative flux, with maximum flux divergence in the photosphere or cooling layer of the convection zone. This group includes the largest number of wavelength points.

The temperature structure of the atmosphere and the group mean photon destruction probabilities are displayed in Figure 2. The cooling layer of the convection zone is located around the height of 0.0 Mm, where the radiative cooling and mean temperature gradient are largest. The group mean destruction probability is given by $1 - \rho_i$, where the group mean scattering albedo ρ_i is given in equation (22).

As the line contribution to the group mean opacity increases (increasing group number), scattering becomes more important, and photons scatter rather than being coupled to the gas via collisions. For a given difference between local temperature and radiation temperature, a smaller destruction probability means a smaller amplitude of the radiative flux divergence as compared to no scattering. The scattering contribution is present also in the first few hundred kilometers into the convection zone (below 0.0 Mm), but it dominates in atmospheric layers above 0.0 Mm for groups 2, 3, and 4.

Horizontal averages of the exact and the approximate radiative heating for the four groups are compared in Figure 3. Here we have used the full approximation given by equations (22), (23), and (24) in the calculation of the

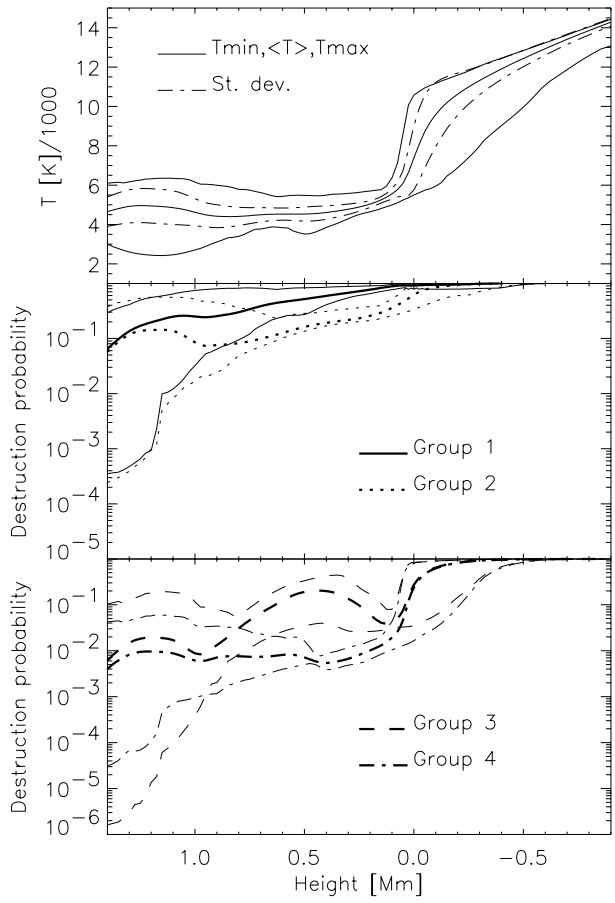

FIG. 2.—*Upper panel:* Mean, maximum, and minimum temperature (*solid lines*) and standard deviation (*dash-dotted lines*) in horizontal planes for the test snapshot. *Lower panels:* Mean (*thick lines*), maximum and minimum (*thin lines*) group mean destruction probabilities in horizontal planes. As the line contribution increases (increasing group number), scattering becomes more important, and photons scatter rather than couple to the gas by collisions. The cooling layer of the convection zone is located around the height of 0.0 Mm, where the radiative cooling is largest.

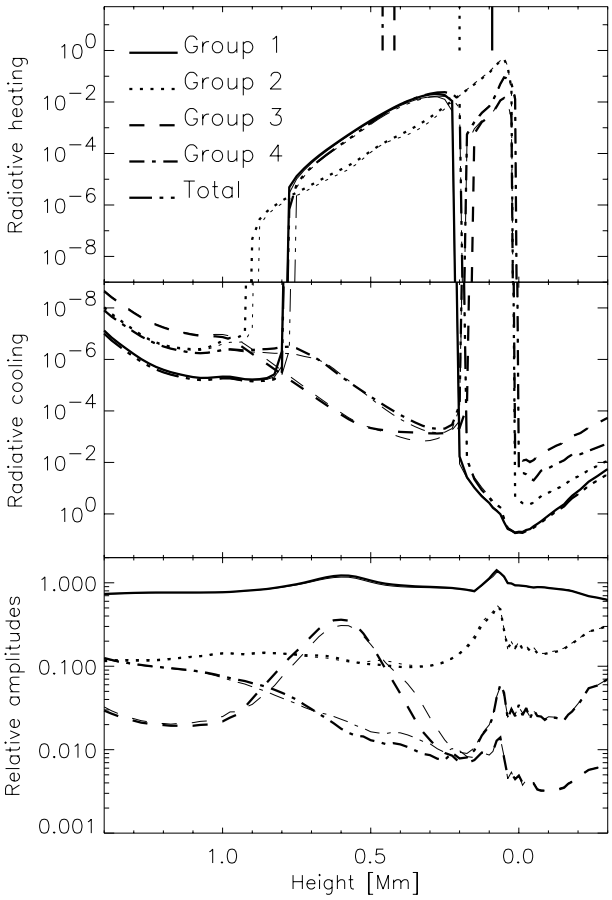

FIG. 3.—*Upper panels:* Horizontally averaged radiative heating per volume unit shown in a bilogarithmic plot. The units are arbitrary. Thick lines are the exact group solutions, while the thin lines are the approximate group solutions. The vertical line segments in the uppermost panel show the heights where the average optical depth per group is unity, as measured along the vertical line. *Lower panel:* Horizontally averaged amplitudes of radiative heating (average absolute value) relative to the amplitude of the exact total heating. Thick lines are the exact amplitude ratios, while the thin lines are ratios from the approximate group solutions.

approximate solution. The horizontal averages (*thin lines*) coincide very well with the horizontal averages of the exact solutions (*thick lines*). The upper panels show cooling below 0.0 Mm in all groups, and heating in groups 2, 3, and 4 immediately above 0.0 Mm.

The lower panel shows the amplitude of the approximate and exact flux divergence (horizontal average of the absolute value) relative to the amplitude of the *total exact* flux divergence, i.e., $\langle|\phi_i^*|\rangle/\langle|\phi_{\rm tot}|\rangle$ and $\langle|\phi_i|\rangle/\langle|\phi_{\rm tot}|\rangle$ (brackets denote horizontal average). We see that the exact relative amplitudes (*thick lines*) coincides very well with the approximate values (*thin lines*).

A sample of the spatial structure is displayed in Figure 4, where we have shown the exact heating per mass unit in all groups as gray-scale images in a vertical slice. Black contours mark locations of zero heating, and lighter shades of gray means positive heating. Gas in layers immediately above the cooling layer is heated in all groups in expanding flow above granules. Granules are seen as curved horizontal structures. As up-flowing gas expands and cools, the temperature falls below the radiation temperature, and the gas is radiatively heated. Note also heating of the cool region

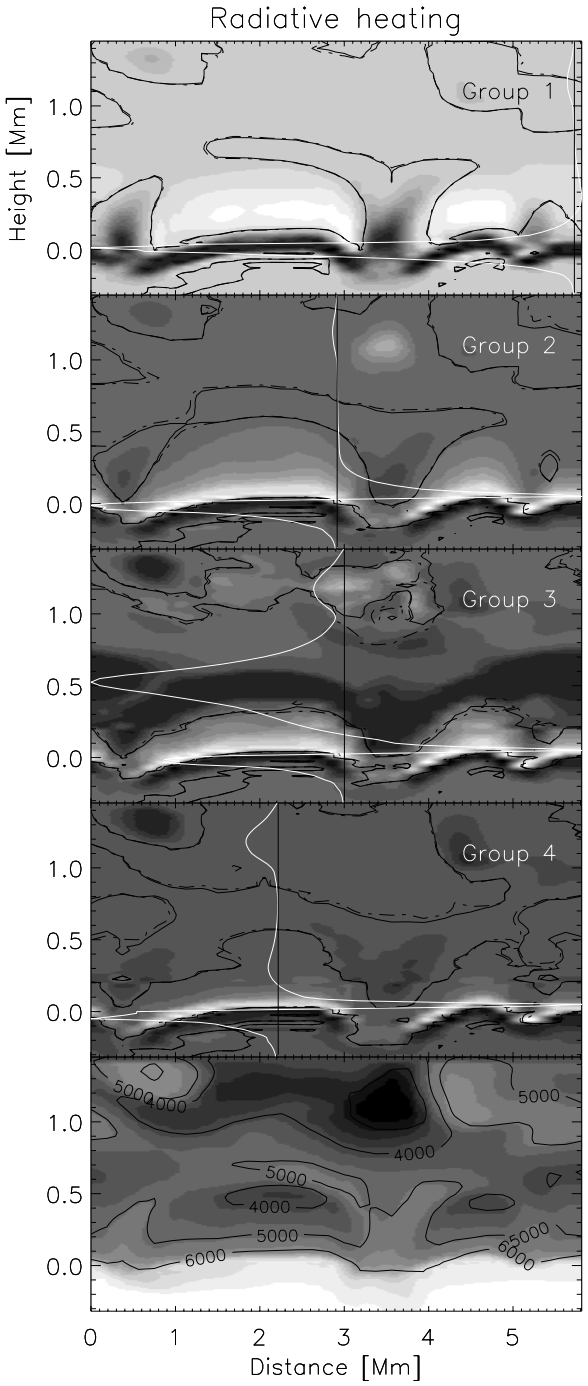

FIG. 4.—Exact group radiative heating per mass unit in vertical slices through the simulation. Full drawn black contours show the level of zero heating. Heating is found at lighter shades of gray, and cooling at darker shades. Dash-dotted black contours show the zero level of the approximate group heating and coincide well with the zero level of the exact heating. White curves are the horizontal averages of the radiative heating per mass unit (normalized to fit the plotting window). Black vertical lines mark the zero level for these curves, and positive values are to the right of the lines. *Lower panel:* Temperature in the same vertical slice. Note the cooling in the granular layer at the height 0.0 Mm, and heating immediately above in all groups, and also heating of the cool region below 3000 K in the chromosphere.

below 3000 K in the chromosphere as radiation energy from below is converted to thermal energy via collisions.

The dash-dotted black contours show the zero level for the approximate heating and coincide well with the zero

level for the exact heating. White curves are horizontal averages per mass unit (normalized to fit the plotting window). The gray-scale plots show that the heating (cooling) contributions can cancel a large part of the cooling (heating) contributions in the horizontal average at a specific depth. This is clearly the case for the curved granular surfaces.

The above comparisons of horizontally averaged heating do not reveal local deviations between approximate and exact solutions since, e.g., excessive heating at a specific height and horizontal region can be canceled by excessive cooling in other regions at the same height. We have therefore computed absolute differences between approximate and exact solutions at each grid point and thereafter calculated the horizontal average of these differences. The relative deviation is found by dividing by the magnitude of the exact radiative heating ϕ_i at the same height: $\langle |\phi_i^* - \phi_i| \rangle / \langle |\phi_i| \rangle$.

The upper panel in Figure 5 shows typically 1%–30% deviations in atmospheric layers, with a peak of 100% deviation in group 3 at 0.35 Mm. The smallest deviations, less than 10%, are found for group 1, which carries the most energy. The total radiative heating is also seen to deviate with less than 10% from exact value because of the dominance of group 1 at all heights. This is the flux-divergence accuracy we can achieve in three-dimensional simulations with the current method.

The lower panel in Figure 5 shows the fraction of grid points that have higher radiative heating than the exact solution. A fraction of 0.5 corresponds to an approximate solution that fluctuates on either side of the exact solution. We see that the approximate solutions have lower values than the exact solutions at 0.3 Mm (immediately above the cooling layer). In the chromosphere, group 1 and 2 have lower values, and group 3 has higher values than the exact solution. Group 4 has approximately the correct values. The total radiative heating is lower than the exact value owing to the domination of group 1. By considering the deviation above, we conclude that the total heating is less than 10% below the exact heating in atmospheric layers.

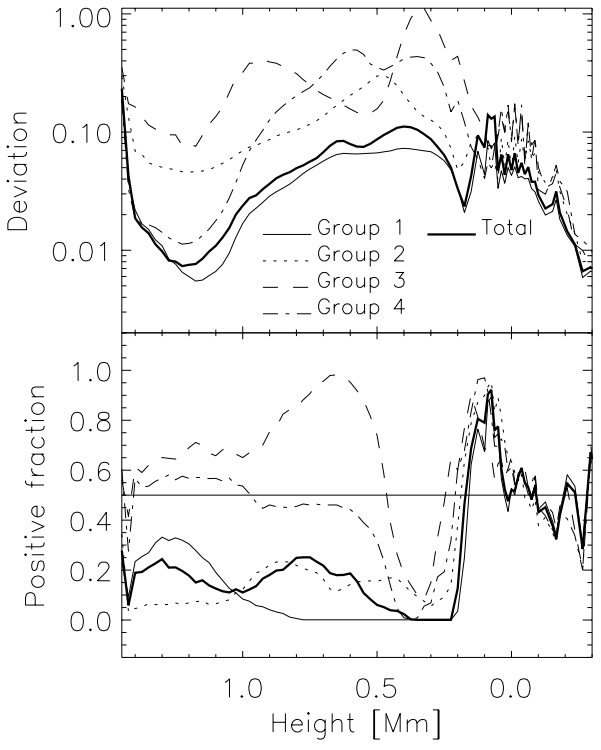

FIG. 5.—Horizontally averaged deviations between approximate and exact group radiative heating. *Upper panel:* Deviations are typically in the range 1%–30%. *Lower panel:* Fraction of grid points in horizontal planes for which the approximate solution is larger than the exact solution.

5.2. *Comparison with a Previous LTE Method*

Here we compare the new method for scattering with the previous LTE method used in the convection simulations of Nordlund and Stein.

5.2.1. *Nordlund's LTE Scheme*

We review this method here; additional information can be found in Nordlund (1982) and Nordlund & Dravins (1990). Nordlund treated the source function in LTE for all groups, $S_i^* = B_i$, and used a scaled opacity for the transport equation, $\chi_i^T = \chi_{i=1}^T 10^{i-1}$, where 10^{i-1} is the typical ratio between monochromatic opacities within group i and the opacity in group 1 at unity optical depth. The binning of wavelengths into groups satisfying these ratios at unity optical depth was performed in the horizontally averaged model. Only $\chi_{i=1}^T$ and B_i were stored in the lookup table, and the flux divergence was calculated as in equation (27) with $S_i^* = B_i$.

Nordlund & Dravins (1990) calculated $\chi_{i=1}^T$ as a corrected standard opacity (Rosseland opacity integrated over continuum opacities only) to include the influence from the depth variation of weak iron lines in optically thin layers:

$$\chi_{i=1}^T = \chi_R^c(\mathrm{3D}) X_{\mathrm{corr}} .$$

χ_R^c(3D) is here the standard opacity, labeled to indicate a three-dimensional structure. X_{corr} was calculated as a function of depth in the horizontally averaged model and weighted between diffusion and streaming regimes:

$$X_{\mathrm{corr}} = \frac{\kappa_{i=1}^{J\mathrm{pp}}}{\chi_R^c} \exp(-2\tau_R^c) + \frac{\chi_R}{\chi_R^c} [1 - \exp(-2\tau_R^c)] .$$

$\kappa_{i=1}^{J\mathrm{pp}}$ includes line plus continuum absorption opacities. The line opacities from the ODF were here treated as pure absorption opacities. χ_R^c is the standard opacity, τ_R^c is the standard optical depth, and χ_R the full Rosseland opacity, all quantities for the horizontally averaged model.

The flux divergence integral (eq. [27]) for group 1 takes this form in the streaming regime:

$$\chi_R^c(\mathrm{3D}) \frac{\kappa_{i=1}^{J\mathrm{pp}}}{\chi_R^c} (B_{i=1} - J_{i=1}^*) ,$$

where

$$\chi_R^c(\mathrm{3D}) \frac{\kappa_{i=1}^{J\mathrm{pp}}}{\chi_R^c}$$

is an approximation to the three-dimensional absorption opacity. This approach approximately excludes the scattering contribution in the flux divergence integral. Note also that $J_{i=1}^*$ is still computed in LTE in this scheme, without iterations.

Details in absorption opacity were not accounted for in groups of numbers higher than 1. Scaling of the opacity in group 1 was assumed to be a sufficient approximation for

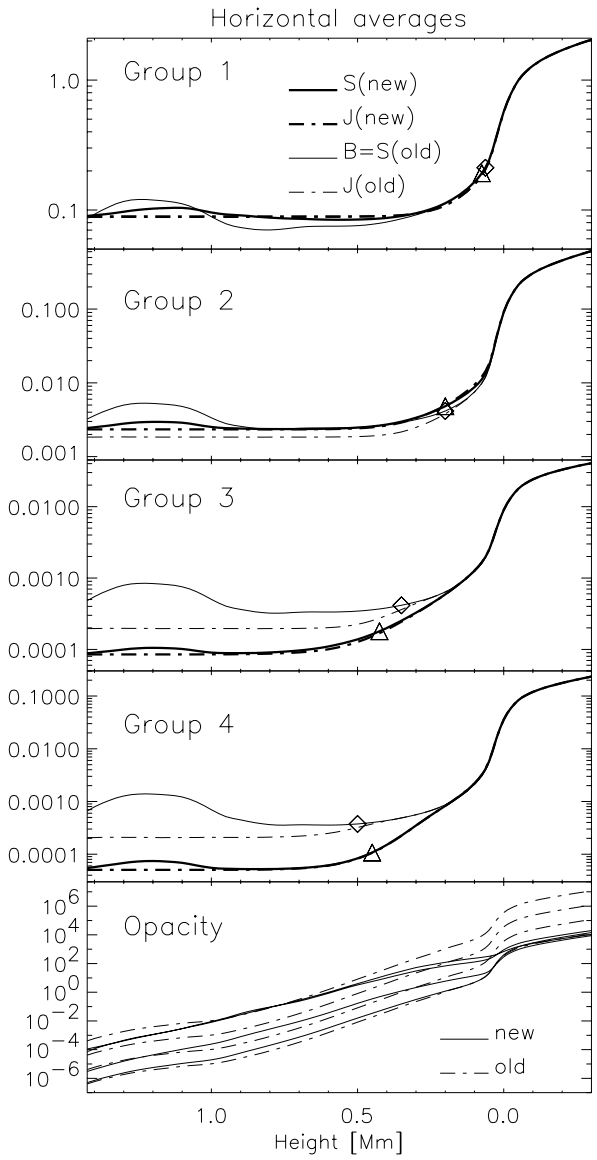

FIG. 6.—Horizontally averaged group mean intensities J and source functions S from the test snapshot. The units are arbitrary, but the scaling is the same for the four first figures. The mean intensities from the new method (new) are closer to the source functions than for the previous LTE method (old). The different values of mean intensities are caused mainly by different source functions, but there is also some influence from differing heights where optical depths are unity. Diamonds and triangles show the heights for where the optical depth is unity. *Lower panel:* Horizontal averages of group mean opacities (arbitrary units). Higher values correspond to higher group numbers. Below 0.0 Mm, all groups have opacities equal to the group mean Rosseland opacity for the new method. Note the scaling by powers of 10 for the "old" opacity.

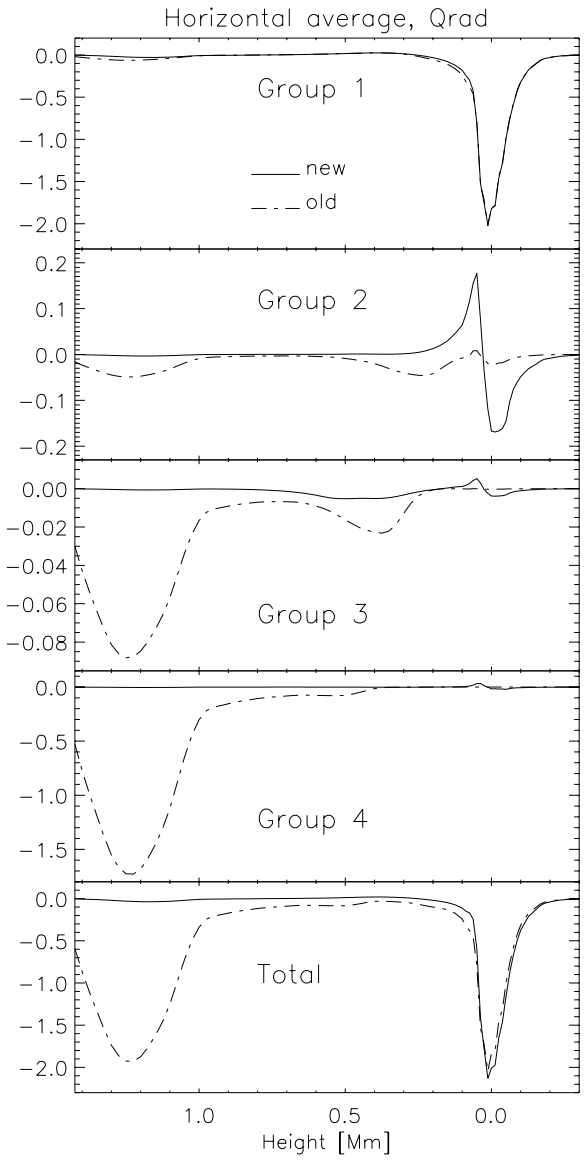

FIG. 7.—Horizontal averages of radiative heating per mass unit. The units are arbitrary, and the scaling is the same for all figures. The amplitude of the flux divergence for the previous LTE method (old) is much larger above 0.3 Mm than for the current method. This effect is caused mainly by the larger differences between the source function and the mean intensity. Around 0.0 Mm, the new method produces larger amplitudes in the sense that hot regions are cooled more and cooler regions are heated more. *Lower panel:* Sum of all groups. The main difference above 1.0 Mm comes from the contribution in group 4.

these opacities. In the new method, we calculate all group mean opacities explicitly, and we also include line scattering.

5.2.2. *Differences in Mean Intensity and Flux Divergence*

Horizontal averages of mean intensities and source functions are compared in Figure 6 for the same snapshot that we have used previously (Fig. 2). We have used the same set of wavelengths per group for LTE and scattering results.

The mean intensities from the new method are closer to the source functions than for the LTE method because of the scattering contribution in the new method. Pure scattering would imply that $J_i^* = S_i^*$. The values of the mean intensities are also differing, mainly because of differences in the source function, and partially because of the different heights for which the optical depths are unity.

Diamonds and triangles show the heights for where the horizontally averaged optical depth $\overline{\tau_i}$ is unity, for previous and current methods, respectively. The mean intensities in optically thin regions are approximately $\langle J_i^* \rangle \simeq \frac{1}{2}\langle S_i^* \rangle$ ($\overline{\tau_i} = 1$). The group mean opacities that determines the optical depths are seen in the bottom panel of Figure 6. The new opacities are higher than the old opacities above 0.3 Mm, except in group 4, where the old opacity has been scaled to higher values over most of the height range. The reason for a lower opacity in group 1 for the LTE method is

that scattering contributions to the opacity are excluded by the $X_{\rm corr}$ factor.

Radiative heating per mass unit is compared in Figure 7. The heating amplitudes for the LTE method is much larger above 0.3 Mm than for the current method. The excessive cooling above 1.0 Mm is caused by the temperature perturbation seen in Figure 2. This effect is caused mainly by the larger difference between the source function and mean intensity. This larger difference is not compensated by the smaller LTE-opacities, such that the amplitudes in heating (cooling) become larger. We note that increased flux divergence amplitudes implies shorter radiative damping time of the waves that cause the temperature perturbations.

In the cooling layer around 0.0 Mm, the case is reversed. The new method produces larger amplitudes in the sense that hot regions are cooled more and cooler regions are heated more. This is because the mean intensities are smoother with scattering than without, hence the differences between local temperature and radiation temperature becomes larger. We should therefore expect smoother temperature gradients in the granular layer. Note that this effect occurs below optical depth unity for groups 2, 3, and 4, i.e., in relatively optically thick layers.

6. SUMMARY

We have developed numerical methods for an approximate solution of the radiative flux divergence in three-dimensional solar/stellar atmosphere simulations. Approximate solutions are obviously necessary in order to reduce the computational costs associated with the time-dependent stellar atmosphere problem, which, in general, involves full NLTE coupling between atomic species. Solar radiation hydrodynamic simulations in three dimensions and two dimensions previously have used strict LTE calculations (e.g., Nordlund 1982; Steffen & Muchmore 1988; Steiner et al. 1998), which works well in the deep photosphere. This work is a step in the direction of relaxing this standard approximation by including scattered radiation.

To make the problem tractable, we have made three fundamental approximations: (1) opacities are still calculated in LTE, (2) coherent and isotropic photon scattering is employed in the source function, and (3) group mean opacities (e.g., Mihalas & Mihalas 1984) substitute for the monochromatic opacity spectrum. This leads to two problems: the definition of the group mean opacities and the solution of the scattering problems in each group.

Group mean scattering, absorption, and total opacities are calculated by a wavelength integration of the transport equation. The opacities have different definitions for optically thin and thick layers. In optically thin layers, we use an approximate radiation field (in the solar case, an estimate of the horizontally averaged radiation field) as a weighting function, except for the group mean absorption opacity, for which we use the exact Planck average. In optically thick layers, we use Planck averages, except for the total opacity. Here we use Rosseland opacities such that the diffusion solution of the transport equation is satisfied. The group mean source function is, by the usual definition, the ratio between emissivity and total opacity. This source function contains an approximate scattering term and an exact contribution from thermal emissivity.

The three-dimensional scattering problems are solved by iteration using a new method based on a one-ray approximation in the angle integral for the mean intensity. The equations to be iterated are tridiagonal matrix equations, one for each ray. For this coherent problem, the method is faster in terms of computer time than the local ALI method (Cannon 1973b; Olson et al. 1986; Hubeny 1992) and Cannon's AQPT method (Cannon 1973a).

We have tested the methods in solar convection-atmosphere simulations (Skartlien 1998; Skartlien et al. 2000), and we need, for each time step, typically 2, 5, 10, and 15 iterations for the four groups we have used to reach an accuracy of about 5×10^{-3} in the source functions. The CPU time used for solving for the radiation scales linearly with the number of angles, grid points, and wavelength groups. Even with approximate treatment of radiation, the CPU time used on hydrodynamics is only marginal compared with that used for the radiation calculations.

We have compared exact wavelength-integrated monochromatic solutions with the corresponding approximate solutions. We find that the total flux divergence obtained from groups deviates less than 10% from the exact solution, with maximum deviation in the upper photosphere. Individual groups that transport less energy deviate typically 30% in atmospheric layers. A factor of typically 100 can be saved in computer time as compared to the monochromatic solution, if the less accurate solution is accepted.

We have compared Nordlund's LTE method (Nordlund 1982; Nordlund & Dravins 1990), which has been used previously in solar and stellar convection simulations, with the current scattering method. The LTE method gives larger amplitudes of radiative heating/cooling in upper atmospheric layers, given the same temperature perturbations. This is caused mainly by the larger differences between the source function (Planck function in LTE) and mean intensity. Chromospheric waves are therefore damped more efficiently in LTE, and wave amplitudes are smaller than with radiation scattering. In deeper, optically thick layers, as in the upper part of the convection zone, the scattering solution produces a spatially smoother mean intensity than the Planck distribution, such that temperature fluctuations are smoothed more efficiently than in LTE.

This work was supported through a grant of computing time (Program for Super-Computing), and by grant 121076/420, "Modeling of Astrophysical Plasmas," from the Norwegian Research Council. Andreas Botnen is thanked for comparisons with his 3D Short Characteristics method and for help with FORTRAN 90 and MPI-programming. Mats Carlsson, Tom Bogdan, and Teresa Palmer are thanked for improving the manuscript. Colorado Research Associates (CoRA) is thanked for hospitality and for providing additional computer resources during this work.

REFERENCES

Botnen, A. 1997, Radiative transfer in 3D, Master's thesis, Inst. Theor. Astrophys. Oslo
Cannon, C. J. 1973a, J. Quant. Spectrosc. Radiat. Transfer, 13, 627
———. 1973b, ApJ, 185, 621
Carlsson, M., & Stein, R. F. 1992, ApJ, 397, L59
———. 1997, ApJ, 481, 500
Feautrier, P. 1964, Comptes Rendus Acad. Sci. Paris, 258, 3189
Gustafsson, B. 1973, Uppsala Astron. Obs. Ann., 5, No. 6
Gustafsson, B., Bell, R. A., Eriksson, K., & Nordlund, Å. 1975, A&A, 42, 407
Hubeny, I. 1992, in The Atmospheres of Early-Type Stars, Lecture Notes in Physics 401, ed. U. Heber & C. S. Jeffery (Berlin: Springer), 377

Jacobi, C. G. 1845, Astron. Nachr., 32, 297
Kiselman, D., & Nordlund, A. 1995, A&A, 302, 578
Kunasz, P. B., & Auer, L. H. 1988, J. Quant. Spectrosc. Radiat. Transfer, 39, 67
Magain, P. 1983, A&A, 122, 225
Mihalas, D. 1978, Stellar Atmospheres (2d ed.; San Francisco: W. H. Freeman)
Mihalas, D., & Mihalas, B. W. 1984, Foundations of Radiation Hydrodynamics (New York: Oxford Univ. Press)
Nordlund, Å. 1982, A&A, 107, 1
———. 1985, in Progress in Stellar Spectral Line Formation Theory, ed. J. E. Beckman & L. Crivellari (Dordrecht: Reidel), 215
Nordlund, Å., & Dravins, D. 1990, A&A, 228, 155
Nordlund, Å., & Stein, R. F. 1990, Comput. Phys. Commun., 59, 119
———. 1991, in Stellar Atmospheres: Beyond Classical Models, ed. L. Crivellari, I. Hubeny, & D. G. Hummer (Dordrecht: Kluwer), 263
Olson, G. L., Auer, L. H., & Buchler, J. R. 1986, J. Quant. Spectrosc. Radiat. Transfer, 35, 431
Rybicki, G. B. 1984, in Methods in Radiative Transfer, ed. W. Kalkofen (Cambridge: Cambridge Univ. Press), 21
Skartlien, R. 1998, Three-Dimensional Modeling of Solar Convection and Atmosphere Dynamics, Ph.D. thesis, Inst. Theor. Astrophys. Oslo
Skartlien, R., Stein, R. F., & Nordlund, Å. 2000, ApJ, in press
Spruit, H. C., Nordlund, Å., & Title, A. M. 1990, ARA&A, 28, 263
Steffen, M., & Muchmore, D. 1988, A&A, 193, 281
Stein, R. F., & Nordlund, Å. 1989, ApJ, 342, L95
Steiner, O., Grossman-Doerth, U., Knoelker, M., & Schussler, M. 1998, ApJ, 495, 468
Van Regemorter, H. 1962, ApJ, 136, 906
Vinsome, P. K. W. 1976, in Proc. 4th Symp. on Reservoir Simulation (Los Angeles: Soc. of Petroleum Engineers), 149